Chemistry Europe
European Chemical Societies Publishing

Supramolecular Chemistry | *Hot Paper*

Building $[U^{IV}_{70}(OH)_{36}(O)_{64}]^{4-}$ Oxocluster Frameworks with Sulfate, Transition Metals, and U^{V}

Ian Colliard and May Nyman*[a]

Abstract: Uranium(IV) oxide clusters, colloids, and materials are designed and studied for 1) nuclear materials applications, 2) understanding the environmental fate and transport of actinides, and 3) exploring the complex bonding behavior of open-shell f-elements. U^{IV}-oxyhydroxsulfate clusters are particularly relevant in industrial processes and in nature. Recent studies have shown that counter-cations to these polynuclear anions differentiate rich structural topologies in the solid-state. Herein, we present nine different structures with wheel-shaped $[U_{70}(OH)_{36}(O)_{64}(SO_4)_{60}]^{4-}$ (U_{70}) linked into one- and two-dimensional frameworks with sulfate, divalent transition metals (Cr^{II}, Fe^{II}, Co^{II}, Ni^{II}) and U^{V}. Small-angle X-ray scattering of these phases dissolved in butylamine reveals differing supramolecular assembly of U_{70} clusters, controlled primarily by sulfates. However, observed trends in transition metal linking guide future design of U_{70} materials with different topologies. Finally, U_{70} linking via U^{IV}-*O*-U^{V}-*O*-U^{IV} bridges presents a rare example of mixed-oxidation-state uranium oxides *without* disorder.

Introduction

Metal-oxo clusters can be considered structural and chemical molecular fragments of metal oxide materials. Framework materials built of metal-oxo clusters (i.e., zeolites[1] and metal–organic frameworks, MOFs[2]) offer a unique approach to controlling and understanding self-assembly, in addition to discovering emergent properties. The ability to isolate the cluster building-blocks allows unprecedented control of materials assembly and unambiguous spectral monitoring of assembly pathways. Metal-oxo clusters can also serve as models for poorly ordered colloids and interfaces, which orchestrate fate and transport of contaminants in the environment.[3]

Metal-oxo clusters of actinides; most commonly uranium, thorium, neptunium, plutonium, offer unique opportunity and prospective in both synthesis and environmental science. These metals have a common tetravalent oxidation state (An^{IV}) and a higher oxidation state that is stabilized as a linear di-oxo complex (i.e., $U^{VI}O_2^{2+}$). An^{IV} assembles into hexameric $An_6O_4(OH)_4$ (An_6, Figure 1 A) cluster units that can be isolated with bidentate bridging ligands ($An_6O_4(OH)_4L_{12}$, L = carboxylate, sulfate, etc.),[4] or further linked into both MOFs and inorganic frameworks.[5] The An_6 unit is also recognized in larger metal-oxo clusters[6] including An_{38},[7] and is an exact building block of AnO_2.[8] Heat or pH change of An_6 solutions promotes facile conversion to soluble AnO_2 colloids.[4a,9] Therefore these molecular clusters are excellent models to understand UO_2 and PuO_2 colloid transport and biomineralization in the environment;[10] in particular because their sulfate and carboxylate ligands are environmentally relevant.

The sulfate-ligated U_6 cluster, that is, $[U_6O_4(OH)_4(SO_4)_{12}]^{12-}$ with its high negative charge and labile sulfate ligands presents opportunity to use counter-cations to direct its assembly into both larger clusters and cluster-based materials, and to mediate its conversion to UO_2 nanoparticles. Yue et al. demonstrated differentiating assembly of U_6-sulfate clusters with the alkalis Na^+ through Cs^+.[4b] We recently demonstrated that higher valence counter-cations (transition metals, TM^{II} and lanthanides, Ln^{III}) yielded unprecedented large clusters featuring the U_6-sulfate building block.[11] With TM^{II}, we isolate a U_{70} ring of U_6 clusters "fused" with U_1-monomers. On the other hand, Ln^{III} isolates U_{84} capsule-like "superatoms" composed of fourteen U_6 clusters, which further link into superlattices. In the ini-

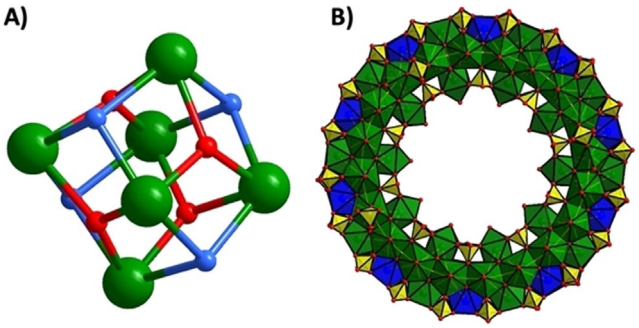

Figure 1. Uranium oxyhydroxo clusters. A) ball and stick representation of the U_6 core with a formula $[U_6(OH)_4(O)_4]^{12+}$, hydroxy is blue, oxo is red, uranium is green. B) Polyhedral representation of U_{70}, the U_6 unit is green, U_1 is blue, sulfate is yellow, oxygens are red spheres.

[a] *I. Colliard, Prof. Dr. M. Nyman*
Department of Chemistry, Oregon State University
Corvallis, OR 97331 (USA)
E-mail: may.nyman@oregonstate.edu

Supporting information and the ORCID identification numbers for the authors of this article can be found under: https://doi.org/10.1002/chem.202002403.

tial study, we introduced the U_{70} topology with Mn^{II} and Zn^{II} counterions. To demonstrate the ubiquity of this approach and to understand the roles of sulfate and transition metals counter-cations in supramolecular assembly, we have now isolated and structurally characterized nine additional **U_{70}** assemblages with Cr^{II}, Fe^{II}, Ni^{II}, and Co^{II} counter-cations. These new structures complete the family of TM^{II}-U_{70} phases from Cr^{II} to Zn^{II}, and we have combined solution-phase small-angle X-ray scattering (SAXS) plus the solid-state structures to identify bonding trends between the U_{70} rings and the TM^{II}-counterions.

Missing from the series is Cu^{II}. Cu plated out via the redox reaction [Eq. (1)];

$$Cu^{II} + U^{IV} \rightarrow Cu^{0} + U^{VI} \quad (1)$$

Fe^{II} also demonstrated redox instability. A minor amount of Fe^{III} in prolonged reactions yielded a unique assembly featuring U^{V} that links the U_{70} rings into a 2D framework via U^{IV}-*O*-U^{V}-*O*-U^{IV} bridges, and represents a rare example of mixed oxidation state uranium compounds without $U^{IV/V}$ disorder. While synthesis and characterization of U^{IV} and U^{VI} oxides and related frameworks is relatively straightforward,[12] U^{V} is more elusive to access and characterize. However, its isolation and characterization is important to understand $U^{IV} \leftrightarrow U^{VI}$ redox behavior in nature,[13] nuclear materials and wastes,[14] and represents potential to discover unusual magnetic states.[15]

Results and Discussion

Structure descriptions

Single crystals of TM^{II}-U_{70} (TM = Cr, Fe, Ni, Co) were grown based on a modified synthesis, recently reported.[11] All nine structures described here crystallize in the *P*-1 space group with unit cell volumes around 12000–15000 Å^3 (Table S1 in the Supporting Information). Briefly, the U_{70} ring (Figure 1B) can be described as ten alternating U_6 clusters and U_1 monomers with a core formula of $[U_{70}(OH)_{36}(O)_{64}]^{116+}$. U–O/OH distances range from 2.05(2) Å–2.63(2) Å (Table S2). Bridging sulfates cap the ring: two sets of ten sulfates line the inside of the ring, and two set of twenty sulfate line the outside, giving a complete basic formula of $[U_{70}(OH)_{36}(O)_{64}(SO_4)_{60}]^{4-}$ (Figure 1B). Additional addenda sulfates (2, 4 or 6), along with TM^{II} for charge balance, define U_{70}-linking patterns, with more sulfates leading to higher-dimensional U_{70} frameworks. In all phases, $[U_{70}(OH)_{36}(O)_{64}(SO_4)_{60}]^{4-}$ plus its addenda sulfates and bound TM^{II} has inversion symmetry, the multiplicity of each site is 2. Phases with 64 sulfates total, $TM_6U_{70}(SO_4)_{64}$, identified for all the studied TM^{II} (including prior-reported Mn and Zn),[11] represents the most abundant phase in the reported syntheses. With longer reaction time, a second minor phase, $TM_4U_{70}(SO_4)_{62}$, co-crystallizes with Cr, Fe and Co counter-cations, whereas the observed minor phase with Ni is $Ni_8U_{70}(SO_4)_{66}$. The three structure types are described below; first in relation to U_{70} linking by sulfates; and second, by the location and bonding of the TM^{II}-counter-cations.

Sulfate linking of U_{70}

$TM_4U_{70}(SO_4)_{62}$ (TM = CR, Fe, and Co) structural motif: Beyond the 60 bridging sulfates of the core U_{70} formulae, additional sulfates provide linkage between U_{70} rings, and define the different structure types. On both faces of the cluster, the U^{IV} centers of the hexamer units are predominantly capped with H_2O ligands. However, in the typical $TM_4U_{70}(SO_4)_{62}$ motif, four of these water molecules are replaced with two sulfates, that further bridge to a neighboring U_{70} in the same manner, so the inter-U_{70} sulfates bridge four U^{IV} (μ_4, pink tetrahedra, U-OSO_3 2.22(5)–2.78(2) Å, Figure 2A). There are three complete U_6-units between the pair of extra bridging sulfates, spanning approximately a third of the ring. Thus, the U_{70} rings are offset, and stack in infinite chains along the *a*-axis.

$TM_6U_{70}(SO_4)_{64}$ (TM = Cr, Fe, Ni, and Co) structural motif: Beyond the two extra sulfates described above, the U_{70} unit of $TM_6U_{70}(SO_4)_{64}$ contains two additional sulfates, terminally bound to a U^{IV} center, on opposite faces of U_{70}, and also related by an inversion center (teal tetrahedra, Figure 2B). These sulfates do not link the U_{70} rings.

With Ni as the counter-cation, the minor phase obtained with prolonged heating is $Ni_8U_{70}(SO_4)_{66}$. In this structural motif, with six addenda sulfates, there are two pairs of μ_4-sulfates on opposite faces and opposite sides of U_{70} (Figure 2C, pink and gray). Rather than linking U_{70} in one-dimension along the *a*-axis, these four sulfates per cluster link the U_{70} rings in two dimensions, approximately in the *ab*-plane. The other two μ_1 sulfates (teal) are terminally bound on opposite sides and faces of the ring. These do not participate in linking U_{70} rings together.

TM^{II}-bonding and linking of U_{70}

The TM^{II} monomers serve as counter-cations, as well as secondary linkers, defining the dimensionality of the framework. The U_{70} rings of $Fe_4U_{70}(SO_4)_{62}$ are decorated with the four Fe^{II}-

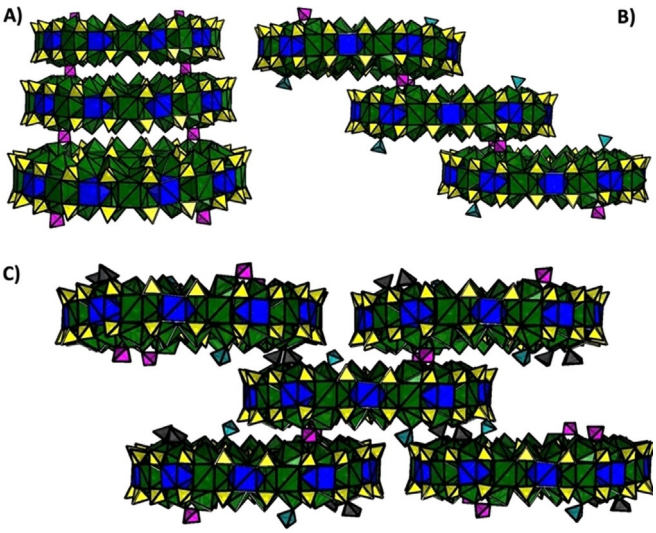

Figure 2. Polyhedral representation of U_{70} frameworks based on sulfate linking. U_6 is green, U_1 is blue, sulfate is yellow. A) $[U_{70}(SO_4)_{62}]^{8-}$, offset chain formation, bridging sulfates are pink. B) $[U_{70}(SO_4)_{64}]^{12-}$, offset chain formation, with additional terminal sulfates in teal. C) $[U_{70}(SO_4)_{66}]^{16-}$, offset 2D formation with additional bridging sulfates in gray.

octahedra, terminally bound to sulfates that bridge the U_1 monomer and U_6, and the octahedral coordination sphere is completed with 5 water molecules (Fe^{II}–OH_2 2.04(2)–2.17(2) Å and Fe^{II}–OSO_3 2.12(1)–2.12(2) Å). They occur in two pairs, each pair is located on adjacent sulfates, and the two pairs are related by an inversion center through the U_{70} ring. The Fe octahedra do not bridge U_{70} rings, so the structure remains one-dimensional, linked only by the sulfates (Figures 3 and S1). $Co_4U_{70}(SO_4)_{62}$ is similar in the lack of connectivity by the TM^{II} counter-cations (Figure S2). There are three Co-sites, one fully occupied, one 75% occupied and the third 25% occupied. Co^{II} sits in the center of very regular octahedra, Co^{II}–OH_2 1.81(7)–2.13(1) Å and Co^{II}–OSO_3 1.99(3)–2.09(1) Å. All Co^{II} are linked to a single U_{70} ring through corner-sharing with a sulfate.

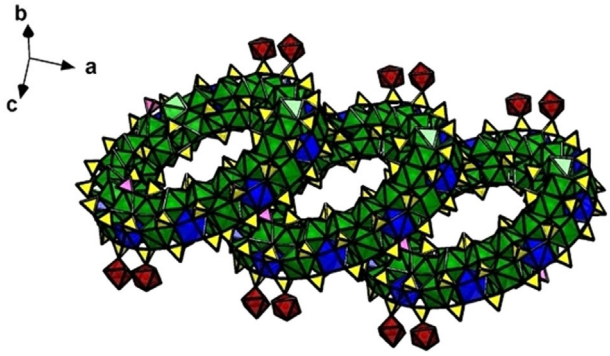

Figure 3. Polyhedral representation of chains in $Fe_4U_{70}(SO_4)_{62}$, U_6 in green, U_1 in blue, sulfate in yellow, oxygens as red spheres, bridging sulfates in pink, and Fe in red-brown.

The rim of each U_{70} ring for $Cr_4U_{70}(SO_4)_{62}$ is decorated by six Cr^{II} sites, with 50–75% occupancy at each of these sites. Cr^{II} exhibits its common Jahn–Teller elongated octahedral distortion (Figure 4a). The long *trans* axial Cr–O bond lengths are 2.26(2)–2.61(2) Å, while the four equatorial Cr–O bond lengths are 1.97(3)–2.18(5) Å. As seen in Figure 4A, the O_3SO-Cr^{II}-OSO_3 link between two adjacent U_{70} clusters are either both long bonds, or one short and one long bond. Therefore, the connectivity by chromium is weak, and this framework (Figures 4B and S3) is also considered 1-dimensional, linked only by the sulfates along the *a*-axis.

Although the $TM_6U_{70}(SO_4)_{64}$ family has more sulfates and more transition metal counterions compared to the $TM_4U_{70}(SO_4)_{62}$, the interconnectivity is not more extensive. This is because some sites are partially occupied, and many bind to only one U_{70} ring via corner-sharing with sulfate, rather than bridge two U_{70} rings. The Cr^{II} of $Cr_6U_{70}(SO_4)_{64}$ has identical coordination as described above, dominated by the elongated Jahn–Teller distortion. The framework of $Cr_6U_{70}(SO_4)_{64}$ is shown in Figure S4. The six Fe^{II} sites in $Fe_6U_{70}(SO_4)_{64}$ range in occupancy from 25–100%, and are both terminally bound and bridging sulfates with bond lengths of Fe^{II}–OH_2 1.91(7)–2.42(3) Å and Fe^{II}–OSO_3 2.04(2)–2.36(7)Å. These sites are exhibited in Figure SI5. Co^{II} and Ni^{II} in their respective $TM_6U_{70}(SO_4)_{64}$ phases show similar bonding and occupancy patterns as described above. The Ni^{II} coordination environments and the $Co_6U_{70}(SO_4)_{64}$ frameworks are shown in Figures S6 and 5, respectively, as representative examples.

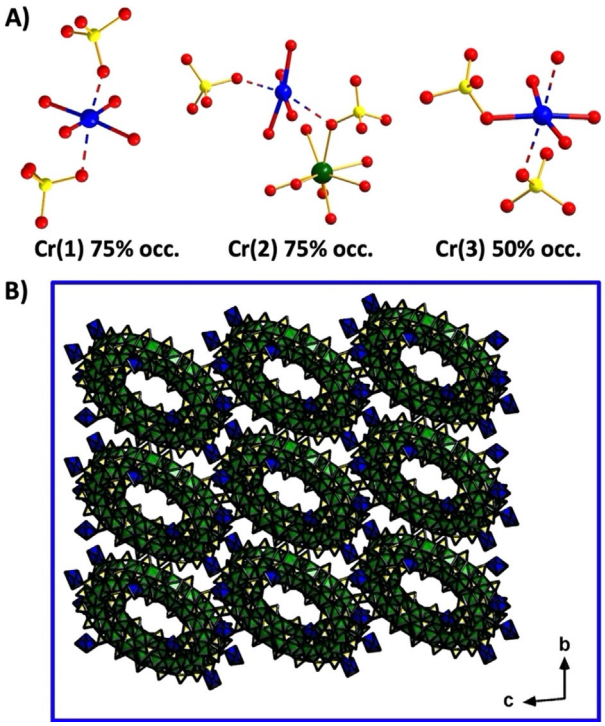

Figure 4. $Cr_4U_{70}(SO_4)_{62}$. A) ball and stick representation of Cr monomers, their occupancy, and bonding showing weak sulfate bonds. B) Polyhedral representation of an extended framework, uranium in green, chromium in blue, sulfate in yellow, oxygen in red.

$Ni_8U_{70}(SO_4)_{66}$ is not only unique in its 2D connectivity via the sulfates, but also by the transition metals. This is the only structure of the nine reported that features true linking of the U_{70} rings through O_3SO-TM-OSO_3 bridges. Figure 6A shows a single U_{70} ring plus all of the 18 Ni^{II} sites to which it connects in the framework (Ni occupancies are 0.25, 0.50 or 0.75). Ni2

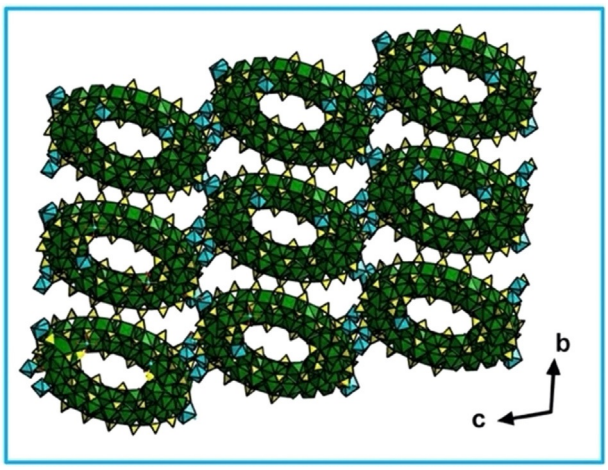

Figure 5. $Co_6U_{70}(SO_4)_{64}$. Polyhedral representation of the extended framework, uranium is green, cobalt is turquoise, sulfate is yellow.

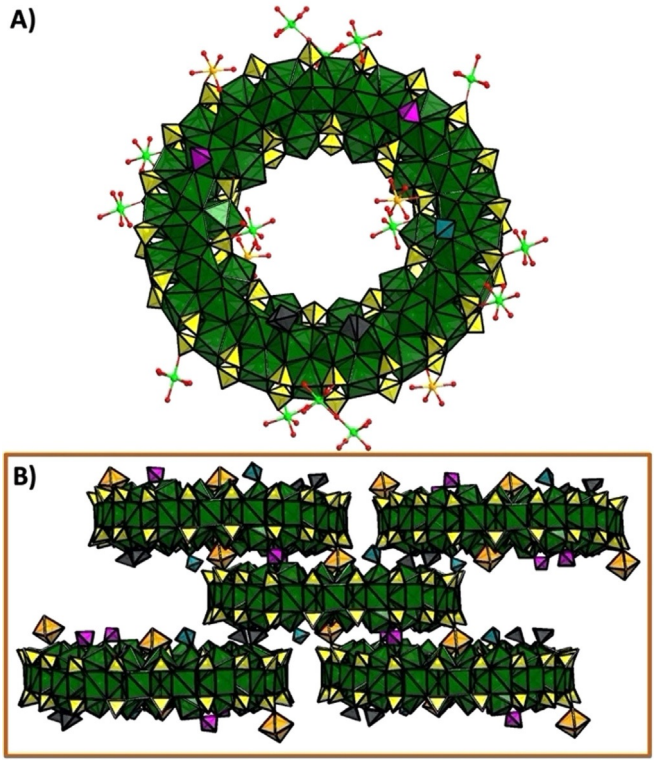

Figure 6. $Ni_8U_{70}(SO_4)_{66}$. A) Polyhedral representation of the U_{70} unit decorated with Ni monomers. B) View of the U_{70} linkage. Uranium is green, nickel in light green, Ni2 (linking U_{70}) is light orange, sulfate is yellow, bridging sulfate is pink and gray.

(0.75 occupancy), highlighted in orange, has relatively short O_3SO-Ni-OSO_3 bond lengths (2.09(1)–2.10(1) Å), and we consider these the TM bridge between U_{70} rings (Figures 6B, S7 and S8). These link the same clusters in the same direction as the bridging sulfates highlighted in Figure 2C (gray), reinforcing the 2D framework of $Ni_8U_{70}(SO_4)_{66}$.

Assembly of TM^{II}-U^{70} in organic media

To further evaluate solution-phase supramolecular assembly trends in TM-U_{70} phases, we have dissolved $TM_6U_{70}(SO_4)_{64}$ in butylamine/THF (3:1), and characterized these solutions by SAXS (Figure 7A, also including prior-reported Zn and Mn analogues). All solutions scatter strongly, owed to both the heavy element uranium and large aggregate sizes (intensity α (atomic number)^2 and radius^6). We performed a size distribution analysis with a cylindrical model (data fitting is shown in Figures S12 to S17), noting that a single U_{70} ring has a diameter measured from the crystal structure of ~35 Å, and a U–U height of 4 Å, or an O–O height of ~10 Å (Figure SI11). Therefore, a solution of isolated U_{70} clusters should have a cylinder diameter of 35 Å, with an aspect ratio (AR) of ~0.1–0.2 (details regarding data fitting and analysis are summarized in the Supporting Information). Considering both the U–U and O–O distance of the cylinder height is important because 1) the sulfates are labile, and 2) the scattering contrast between the capping ligands and the solvent is low, and the majority of the scattering comes from the U-O core of U_{70}.

Figure 7B plots the distribution of cylinder diameters, where peak area and FWHM can be correlated, respectively with solubility and polydispersity (Table 1). Although we targeted equivalent concentration solutions, all solutions were filtered prior to measurement, some with visible particles. TM-U_{70} with Cr, Co, and Ni all have the same main species diameter of ~42 Å and a cylinder height of ~20 Å, consistent with the disulfate-bridged U_{70} dimer illustrated in Figure 7c, and also highlighted in Figures 2B and S11. In contrast, analysis of the Fe-U_{70} scattering indicates species with dimensions a little smaller than an isolated cluster, and the scattering curve is the most featureless. For example, it is missing the two plateaus between $q = 0.18$ and 0.80 $Å^{-1}$. As noted, Fe^{II} oxidizes more readily than the other studied TM^{II}, leading to the $U^{V/IV}$ assembly that is discussed below, and the weaker scattering data may be due to

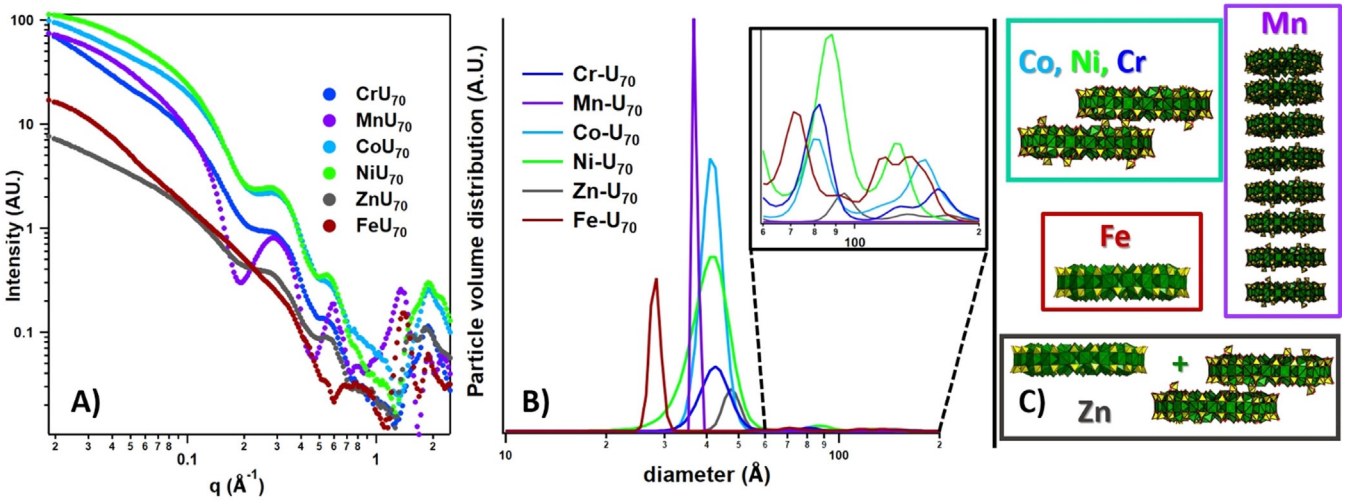

Figure 7. Small angle X-ray scattering and analysis. A) Experimental scattering curves for butylamine/THF solutions of TM-U_{70}. B) Size-distribution analyses; the inset shows an expanded view for diameters of 60–200 Å, revealing the minor population of larger aggregates. C) Major U_{70} assemblies present in the different TM-U_{70} solutions, based on size-distribution analyses (see also Table 1). Analyses indicates the following species: predominantly U_{70} monomers for Fe-U_{70}, mixture of U_{70} monomers and offset dimers for Zn-U_{70}, predominantly offset U_{70} dimers for Co, Ni and Cr U_{70}, eclipsed stack of ~8 U_{70} for Mn.

Table 1. Summary of SAXS data analysis of TM^{II}-U_{70} in butylamine/THF.

		Parameters for size distribution fit of SAXS data		Analysis of size distribution peak	
TM^{II}	AR[a]	Diameter [Å]	Height [Å]	Peak area	FWHM[b]
Cr	0.525	42.3	22.2	18	9.9
Mn	3.3	37.0	122.1	6.4	1.5
Fe	0.125	28.0	4.0	3.5	2.5
Co	0.425	41.4	17.6	17.5	7.3
Ni	0.525	41.2	21.6	18	12
Zn	0.225	47.6	10.7	2.4	6.5

[a] AR = aspect ratio, [b] FWHM = full width at half maximum.

partial dissociation of these clusters. As presented prior,[11] Mn-U_{70} has the most distinctive scattering curve, showing an eclipsed stacking of the U_{70} units (ca. $(U_{70})_8$, shown in Figure 7C).

As observed in the solid-state structures, sulfates play the major role in linking U_{70} into offset stacks (Figure 2), while the TM-counterions play a lesser role. Based on SAXS analysis, this dominant face-to-face, offset stacking is retained in the organic media, which is a very different medium than the aqueous synthesis solution. We can distinguish between eclipsed stacking and offset stacking by the respective presence and absence of a strong oscillation. This oscillation is observed for Mn-U_{70}, between $q = 0.2$ and 0.5 $Å^{-1}$ in Figure 7A, whereas the Cr, Co, Ni, and Zn-U_{70} solutions show a weaker oscillation, or a plateau feature. To further illustrate this point, we compare the simulated scattering from an eclipsed and staggered dimer (Figure S18) to the experimental scattering for Cr, Co, and Ni. Not only does the oscillation indicate a staggered stack rather than an eclipsed stack, but the "shallower" Guinier region of for the staggered stack is a closer match to the experimental scattering. The upward slope at lower q for the experimental curves indicates a small degree of further aggregation of the dimers. Scattering from these aggregates is also observed in the size distribution profiles between diameter = 60–100 Å (inset, Figure 7B).

One of the major questions that arises is, why is offset stacking and linking always favored from self-assembly in water (observed in all reported structures), and upon dissolution in organic media? It is likely not controlled by favored positions of the linking sulfates in the ring. This is because sulfates replace capping water molecules without distorting the ring, so the positions are not necessarily unique. In fact, they are likely labile in solution. Inspecting other prior-reported wheel-cluster lattices; that is, Pd_{84},[16] Mn_{70},[17] and Mo_{154},[18] capped with acetate or $O^{2-}/OH^{-}/H_2O$, we note that eclipsed stacking is far more common than offset stacking. Of these prior-reported wheel-shaped clusters, they do not have capping groups that provide the opportunity for linking between clusters, as sulfate does. As can be viewed in Figure 2B, the offset from perfectly eclipsed U_{70} rings is approximately the radius of the cluster. In other words, the center of each cluster is capped by the rim of the neighboring U_{70} wheels directly above and below, further highlighted in Figure SI10. With the relatively small charge of the large U_{70} ring (−12 in the most frequently observed phase) and the multivalent counter-cations, there are few extra framework species to fill lattice void spaces. Therefore, we presume the clusters link in this manner, in both the solid-state and upon dissolution in organic media, to maximize interaction and minimize energetically unfavorable, accessible void space.

To understand the minor role of TM^{II} in U_{70} linking, in particular why Mn^{II} uniquely achieves an eclipsed form in organic media, we have summarized some pertinent parameters for each transition metal and its bonding behavior in the most commonly observed phase, $TM_6U_{70}(SO_4)_{64}$ (Table 2). Across the 3d series of $TM_6U_{70}(SO_4)_{64}$ phases, there is a distinct increase H_2O–TM ligation, and a corresponding decrease in O_3SO–TM ligation, where nearly all TM^{II} are octahedral or distorted octahedral. We attributed this previously[11] to decreasing covalency of the O_3SO–TM bond across the series,[19] and therefore favored for TM^{II} earlier in the 3d series. However, if this periodic trend drives the TM^{II} linkage of U_{70} in organic media, then we would expect Cr^{II} to likewise exhibit similar behavior, leading to eclipsed stacks.

Other factors are ionic radii and complexation behavior of TM^{II}, and Mn^{II} stands out in both regards. We need to make some assumptions with respect to the d-electron configurations as a H_2O/sulfate-ligated complex (i.e., linking U_{70}) and as an amine complex (solvated, unavailable for linking U_{70}). In the spectrochemical series, amine is considered a "strong" ligand (promoting large stabilization of e_g orbitals and low spin of d-electron configurations), and sulfate is considered a "medium" ligand. With these caveats, the ionic radii are summarized in Table 2. Mn^{II} has both the largest radius of the studied transition metals and the weakest complexation behavior, both properties due to the half-filled d-shell. For example, calculated complexation constants (log(K)) for monoamines[20] are also compiled in Table 2. Mn^{II} has the lowest, a value akin to alkaline earth cations. Perhaps the larger radius allows for higher connectivity and interaction with the U_{70}. Furthermore, Mn^{II} has a lower affinity to complex with N-donor ligands in the studied organic solutions. As a result, Mn^{II} has a higher probability to interact with U_{70}, presumably orchestrating the assembly of the $(U_{70})_8$ eclipsed stack. As the ionic radius decreases, and affinity to complex with butylamine increases, the ability

Table 2. Ionic radii and amine complex stability[20] for TM^{II} in $TM_6U_{70}(SO_4)_{64}$ phases, plus summary of the TM^{II} coordination environments in solid-state structures.

$TM_6U_{70}(SO_4)_{64}$	Ionic	log K[a]	Number of $TM^{II}O_6$ polyhedra with $H_2O/(SO_4+H_2O)$ ligation		
	radius [Å][21]	amine	4/6 H_2O	5/6 H_2O	6/6 H_2O
Cr	0.73[c]	NA[b]	6	0	0
Mn	0.83[d]	1.32	6	0	0
Fe	0.61[e]	1.68	1.5	4.5	0
Co	0.65/0.75[f]	1.97	2	4	0
Ni	0.69	2.02	0.5	4.5	1
Zn	0.74	2.13	0	2.5	3.5

[a] calculated complexation constant for monoamine[20] [b] not available [c] assume low spin due to observed Jahn-Teller distortion in solid state [d] high spin,[11] [e] high spin, [f] low spin/high spin.

for the TM^{II} monomers to form large assemblies in solution diminishes. Therefore, assembly driven by sulfate-linking dominates, which, according to solid-state structures, is predominantly offset ring stacking.

Finally, an exceptional U_{70} phase is isolated from prolonged heating of Fe^{II}-U_{70} reaction solutions, denoted $Fe(U^{V}O_2)_2U_{70}(SO_4)_{62}$. The presence of traces of Fe^{III} accelerates the oxidation of uranium, leading to an architecture of U_{70} linked by a U^{V} dimer unit. The $Fe(U^{V}O_2)_2U_{70}(SO_4)_{62}$ framework is composed of the $[U_{70}(SO_4)_{62}]$ units linked by two sulfates along the *a*-axis, as shown in Figure 2A. Similar to the linking of the $[U_{70}(SO_4)_{66}]$ units, these U_{70} chains are further assembled into sheets, but by the U^{V} dimer, rather than additional sulfates as shown in Figure 2C. The framework features a unique U^{IV}-*O*-U^{V}-*O*-U^{IV} bonding that interconnects the entire sheet along the *ab*-plane, illustrated in Figure 8B. The attribution of the ligands (H_2O, OH^-, O^{2-}) and designation of U^{V} were determined by both bond valence sum (BVS) by using the parameters of Burns,[22] as well as the geometry of the polyhedra (Table 3). The U^{V}-*O*-U^{IV} bridges of the dimer are formed by replacing H_2O caps of side-by-side U^{IV} with O^{2-}, within a U_6 unit of U_{70}. These U^{IV}-O^{2-} bond distances are 2.31(2)–2.33(3) Å, approximately 0.5 Å shorter than a typical U^{IV}-OH_2 bond length in U_{70}. The resulting 2D assembly can be formulated as $[(U^{V}O_2(OH))_2U_{70}(SO_4)_{62}]_n^{8n-}$, Figure 8C. The U^{V} dimer (with inversion symmetry) links to U_{70} via a U^{V}–O distances of 1.89(3) and 1.90(2) Å, and with an O-U^{V}-O angle of 175.86°. The two U^{V} centers are bridged by two hydroxy ligands, U^{V}—OH 2.37(3) and 2.42(2) Å. The pentagonal bipyramid U^{V} geometry is completed with three additional aqua ligands in the equatorial plane. The ligand BVS's without considering protons (not located in the structure) very clearly designate their attribution: OH^- is ~1, H_2O are ~0.4–0.5; O^{2-} are ~1.95 (Table 3). The BVS for this uranium site is almost exactly 5 (Table 3). The BVS along with the lengthened axial U—O bonds (U^{VI}-O_{axial} is typically 1.75–1.85 Å) and slightly "bent" O-U-O axial angle leaves no ambiguity concerning the pentavalent uranium designation. Finally, the Fe^{II} monomers display similar coordination as other described phases (Figures 8A and S9).

Table 3. Bond valence sum assessment of linking uranium dimer of $Fe(U^{V}O_2)_2U_{70}(SO_4)_{62}$.

Atom 1	Atom 2	Bond length [Å]	Bond valence[a] and sum	Attribution
U36	O197	2.368	0.543	
	O197	2.420	0.491	
	O195	1.899	1.340	
	O196	2.483	0.435	
	O19	2.558	0.376	
	O210	2.387	0.523	
	O208	1.889	1.366	
			5.074	U^{V}
O197	U36	2.368	0.543	
	U36	2.420	0.491	
			1.034	OH^-
O195	U36	1.899	1.340	
	U19	2.307	0.611	
			1.951	O^{2-}
O196	U36	2.483	0.435	
			0.435	H_2O
O19	U36	2.558	0.376	
			0.376	H_2O
O210	U36	2.387	0.523	
			0.523	H_2O
O208	U36	1.889	1.366	
	U23	2.334	0.580	
			1.946	O^{2-}

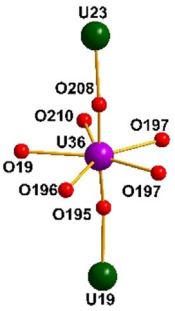

[a] BVS parameters: $R_{ij} = 2.051$, $b = 0.519$.[22]

Unfortunately, $Fe(U^{V}O_2)_2U_{70}(SO_4)_{62}$ has only been synthesized as a minor secondary co-crystallite, due to the difficulty in controlling uranium oxidation and the relative instability of U^{V}. Importantly, it is a rare example of a mixed oxidation state uranium compound without disorder of hetero-valent uranium. U^{V} coordination geometry represents a transition between U^{IV} (8–9 coordinate, spherical ligand field) and U^{VI} (strongly directional ligand field featuring the linear UO_2^{2+} uranyl, 6–8 coordinate), leading to mixed $U^{IV/V}$ and $U^{V/VI}$ occupancy in crystalline lattices and ambiguity in characterization. Examples of mixed-valence oxides (both ordered and disordered) include 1) $Cs_2K(UO)_2Si_4O_{12}$ featuring corner-linked $U^{IV/V}$,[23] 2) $(Rb,Cs)_3(U_2O_4)(Ge_2O_7)$ featuring corner-linked U^{V} and U^{VI},[24] 3) $[Na_7U^{IV}O_2(U^{V}O)_2(U^{V/VI}O_2)_2Si_4O_{16}]$ with corner-linked U^{IV} and edge-linked U^{V}-$U^{V/VI}$,[25] and 4) $(Rb,Cs)_2Na[(U^{V,VI}O_2)_2(Si_2O_7)]$ with corner-linked U^{VI} and U^{V}.[26] Most of these phases are open framework, and corner linking of the mixed-valence polyhedra is more common than edge linking. This can be rationalized by the flexibility of such frameworks, accommodating the distortion and disorder of mixed-valence sites. Even rarer is mixed-valence U-oxo cluster molecules, perhaps for the very reason that clusters often feature edge-sharing polyhedra in compact structures. To our knowledge, there is only one prior example; a $U^{IV}{}_3U^{VI}{}_3O_8$ hexamer capped by three tungsten polyoxometalate fragments.[27] In summary, $Fe(U^{V}O_2)_2U_{70}(SO_4)_{62}$ represents a rare example of a hybrid cluster-framework material with ordered hetero-valent uranium.

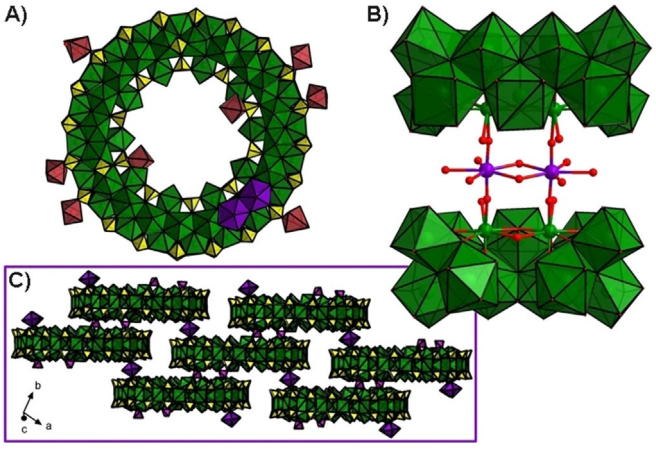

Figure 8. $Fe(U^{V}O_2)_2U_{70}(SO_4)_{62}$. A) Polyhedral representation of U_{70} emphasizing Fe and U^{V} dimer bonding positions on the U_{70} ring. B) Representation of the U^{V} dimer and its connectivity to the U_{70} ring. C) Framework formation showing extended connectivity by the sulfate and U^{V}. U^{IV} is green, U^{V} is purple, bridging sulfate is pink, sulfate is yellow, Fe is brown-red, oxygen is red spheres.

Conclusions

We have presented here an entire series of U^{IV}_{70}-sulfate cluster anions, assembled into intricate frameworks by sulfate bridging, and bridging of the TM^{II} counterions. By assessing the solid-state structures and solution-phase X-ray scattering, we have concluded that the sulfates play the major role in cluster-linking. Unlike other reported wheel-shaped clusters, U_{70} assembles into lattices with offset, rather than eclipsed stacking. We attribute this to the ability of the sulfates to link the clusters in a manner that maximizes interaction and diminishes free void space. Sulfate-linked U_{70} dimers dominate solutions of all TM^{II}-U_{70} phases, with the exception of Mn^{II}-U_{70}. Mn^{II} appears to enable eclipsed linking of large U_{70} stacks. Future studies will include adding different metal ions and clusters to these TM^{II}-U_{70} solutions, to promote differentiating supramolecular assemblies, leading to crystallization of U_{70}-based materials with large pores and channels. Despite careful control to prevent $U^{IV} \rightarrow U^{VI}$ oxidation, we fortuitously isolated a Fe^{II}-U^{V}-linked U_{70} phase, a rare example of a mixed-oxidation-state uranium oxide compounds without U^{IV}–U^{V} site disorder. This provides the incentive to improve control over redox reactions in U^{IV}–sulfate cluster syntheses, which could lead to rich topological diversity and electronic properties.

Experimental Section

Synthesis

Materials: $UO_2(CH_3COO)_2$, concentrated H_2SO_4 (98% Macron Fine Chemicals), $CrCl_3$ (99.0%, Sigma–Aldrich), Zn (99.0%, Sigma–Aldrich), Hydrochloric acid (Macron Fine Chemicals), $Na(CH_3COO)$ (99.0%, Sigma–Aldrich), $Fe(CH_3COO)_2.4H_2O$ (99.0%, Sigma–Aldrich), $Co(CH_3COO)_2$ (99.0%, Sigma–Aldrich), $Ni(CH_3COO)_2.2H_2O$ (99.0%, Sigma–Aldrich), Tetrabutylammonium Chloride (>97%, Sigma–Aldrich) were all used as received. Millipore-filtered water with a resistance of 18.2 MΩ·cm was used in all reactions.

CAUTION! ^{238}U is an alpha-emitting radio-isotope. An appropriate safety protocol should be followed when handling radioactive material.

$TM_6U_{70}(SO_4)_{64}$ (TM = Cr, Fe, Co, Ni) was synthesized by modifying the previously reported synthesis for the TM-U_{70}.[11] 100 mg of $U(SO_4)_2$ (0.23 mmol) is dissolved in 500 μL of H_2O in a 2 mL vial. To the solution, 50 mg of TM^{II} acetate (0.204 mmol) is added (TM = Fe, Co, Ni). For $Cr_6U_{70}(SO_4)_{64}$, we utilized 65 mg (0.265 mmol) of $Cr_2(CH_3COO)_4.2H_2O$[28] as the Cr^{II}-source. Additionally, 200 μL of 1 g mL^{-1} TBACl solution in H_2O is added to each reaction. The vial is then placed in a sand bath and heated in an oven at 75 °C for 2–3 days. During the hydrothermal process, crystals of $TM_6U_{70}(SO_4)_{64}$ grow (Cr after two days, Fe, Co, Ni after 3). The crystals are then filtered out and washed with 2 mL of 0.5 M HCl, followed by 2 mL of H_2O. Approximate yields after 3 days of heating were 75% (Cr), 70% (Fe), 80% (Co), 65% (Ni).

The additional minor phases co-crystallize with more extensive heating. $TM_4U_{70}(SO_4)_{62}$ (TM = Cr, Fe, Co) and $TM_8U_{70}(SO_4)_{66}$ (TM = Ni) could be obtain as a minor phase after five days or longer of heating. Both phases have rectangular prism prismatic shaped crystals, making visual differentiation difficult. The additional phases were identified by rigorous unit cell checking. Empirical observations suggest the minor phases comprise less than 5% of total yield.

Crystallographic studies: Single crystal data for $TM_6U_{70}(SO_4)_{64}$ (TM = Cr, Fe, Co, Ni), $TM_4U_{70}(SO_4)_{62}$ (TM = Cr, Fe, Co), $TM_8U_{70}(SO_4)_{66}$ (TM = Ni), and $Fe(U^{V}O_2)_2U_{70}(SO_4)_{62}$ were collected at 173 K on a Rigaku Oxford SynergyS equipped with a PhotonJet S Cu source (λ = 1.54178 Å) and hyPix-6000HE photon counting detector. All images were collected and processed using CrysAlis^{Pro} Version 171.40_64.53 (Rigaku Oxford Diffraction, 2018).[29] After integration, both (analytical) absorption and empirical absorption (spherical harmonic, image scaling, detector scaling) corrections were applied.[30] All nine structures were solved by Intrinsic Phasing method from SHELXT program,[31] developed by successive difference Fourier syntheses, and refined by full-matrix least square on all F^2 data using SHELX[32] via OLEX2 interface.[33] For more information of refinement, solvent mask, modeling of disorder, and Bond Valence Sum, see the Supporting Information. Crystallographic information and additional structural information can are also provided in the Supporting Information. Deposition numbers 1998606 ($Co_4U_{70}(SO_4)_{62}$), 1998607 ($Cr_4U_{70}(SO_4)_{62}$), 1998608 ($Co_6U_{70}(SO_4)_{64}$), 1998609 ($Fe(UO_2)_2U_{70}(SO_4)_{62}$), 1998610 ($Cr_6U_{70}(SO_4)_{64}$), 1998611 ($Fe_4U_{70}(SO_4)_{62}$), 1998612 ($Fe_6U_{70}(SO_4)_{64}$), 1998613 ($Ni_6U_{70}(SO_4)_{64}$), and 1998614 ($Ni_8U_{70}(SO_4)_{66}$) contain the supplementary crystallographic data for this paper. These data are provided free of charge by the joint Cambridge Crystallographic Data Centre and Fachinformationszentrum Karlsruhe Access Structures service www.ccdc.cam.ac.uk/structures.

Small angle X-ray scattering: SAXS data were collected on an Anton Parr SAXSess instrument utilizing $Cu_{K\alpha}$ radiation and line collimation. Data were recorded on an image plate in the range of 0.08–2.5 Å^{-1}. Sample to image plate distance of 26.1 cm. Solutions were measured in 1.5 mm glass capillaries. Tetrahydrofuran/Butylamine (1:3) was used as the background, and scattering was measured for 30 minutes. SAXSQUANT software was used for data collection and processing (normalization, primary beam removal, and background subtraction. The cylindricalAR fits of the scattering data were carried out utilizing size distribution in the IRENA macros within IGOR Pro,[34] and details and results of these fittings are found in the Supporting Information. Simulated scattering curves of U_{70} and relevant aggregates were generated using SolX by using structural files (.xyz) containing the selected portion of the structure with no symmetry operations. Simulation of various stacking arrangement and aggregations of the structures were creating using Avogadro.[35] The TM-U_{70} solutions were made by dissolving 30 mg of TM-U_{70} crystals in a solution of 1 mL of THF/butylamine (1:3). The solutions were then heated at 35 °C for 1 h. The solutions were filtered prior to placing in the capillary tube for analysis, using a 0.45 μm nylon syringe filter.

Fourier-transform infrared spectroscopy: IR spectra were recorded in attenuated reflectance mode (ATR) using a Thermo Scientific Nicolet iS10 FTIR spectrometer. The spectra and table of sulfate peaks assignments Supporting Information.

Thermogravimetric analysis: TGA analysis was performed on SDT Q600 TA Instrument in the range of 25–800 °C under argon flow, and at a heating range of 10 °C min^{-1}. TGA analysis was conducted to determine the number of solvent waters, see the Supporting Information.

Acknowledgements

This work was supported by the Department of Energy, National Nuclear Security Administration (NNSA) under Award Number DE-NA0003763. We acknowledge the Murdock Chari-

table Trust (Grant No. SR-2017297) for acquisition of the single-crystal X-ray diffractometer.

Conflict of interest

The authors declare no conflict of interest.

Keywords: actinides · polyanions · polyoxometalates · SAXS · supramolecular · uranium

[1] J. M. Fedeyko, D. G. Vlachos, R. F. Lobo, *Langmuir* **2005**, *21*, 5197 – 5206.

[2] a) J. H. Cavka, S. Jakobsen, U. Olsbye, N. Guillou, C. Lamberti, S. Bordiga, K. P. Lillerud, *J. Am. Chem. Soc.* **2008**, *130*, 13850 – 13851; b) B. Nohra, H. El Moll, L. M. R. Albelo, P. Mialane, J. Marrot, C. Mellot-Draznieks, M. O'Keeffe, R. N. Biboum, J. Lemaire, B. Keita, L. Nadjo, A. Dolbecq, *J. Am. Chem. Soc.* **2011**, *133*, 13363 – 13374; c) D. Y. Du, J. S. Qin, S. L. Li, Z. M. Su, Y. Q. Lan, *Chem. Soc. Rev.* **2014**, *43*, 4615 – 4632.

[3] a) Q. Xue, Y. Ran, Y. Z. Tan, C. L. Peacock, H. H. Du, *Chemosphere* **2019**, *224*, 103 – 110; b) J. A. Soltis, M. E. McBriarty, O. Qafoku, S. N. Kerisit, E. Nakouzi, J. J. De Yoreo, E. S. Ilton, *Environ. Sci. Nano* **2019**, *6*, 3000 – 3009; c) F. F. Marafatto, B. Lanson, J. Pena, *Environ. Sci. Nano* **2018**, *5*, 497 – 508; d) J. Hua, C. S. Liu, F. B. Li, Z. K. Zhu, Z. Q. Wei, M. J. Chen, T. Gao, G. H. Qiu, *ACS Earth Space Chem.* **2019**, *3*, 895 – 904.

[4] a) N. A. Vanagas, J. N. Wacker, C. L. Rom, E. N. Glass, I. Colliard, Y. S. Qiao, J. A. Bertke, E. Van Keuren, E. J. Schelter, M. Nyman, K. E. Knope, *Inorg. Chem.* **2018**, *57*, 7259 – 7269; b) Z. Yue, X. Guo, M. L. Feng, Y. J. Lin, Y. Ju, X. Lin, Z. H. Zhang, X. Guo, J. Lin, Y. Y. Huang, J. Q. Wang, *Inorg. Chem.* **2020**, *59*, 2348 – 2357; c) C. Hennig, S. Takao, K. Takao, S. Weiss, W. Kraus, F. Emmerling, A. C. Scheinost, *Dalton Trans.* **2012**, *41*, 12818 – 12823; d) G. Lundgren, *Ark. Kemi* **1953**, *5*, 349 – 363; e) S. Takao, K. Takao, W. Kraus, F. Emmerling, A. C. Scheinost, G. Bernhard, C. Hennig, *Eur. J. Inorg. Chem.* **2009**, 4771 – 4775.

[5] a) J. Lin, G. B. Jin, L. Soderholm, *Inorg. Chem.* **2016**, *55*, 10098 – 10101; b) C. Falaise, J. S. Charles, C. Volkringer, T. Loiseau, *Inorg. Chem.* **2015**, *54*, 2235 – 2242; c) C. Falaise, K. Kozma, M. Nyman, *Chem. Eur. J.* **2018**, *24*, 14226 – 14232; d) N. P. Martin, J. Marz, H. Feuchter, S. Duval, P. Roussel, N. Henry, A. Ikeda-Ohno, T. Loiseau, C. Volkringer, *Chem. Commun.* **2018**, *54*, 6979 – 6982.

[6] a) M. Dufaye, N. P. Martin, S. Duval, C. Volkringer, A. Ikeda-Ohno, T. Loiseau, *RSC Adv.* **2019**, *9*, 22795 – 22804; b) B. Biswas, V. Mougel, J. Pécaut, M. Mazzanti, *Angew. Chem. Int. Ed.* **2011**, *50*, 5588; *Angew. Chem.* **2011**, *123*, 5702.

[7] a) N. P. Martin, C. Volkringer, N. Henry, X. Trivelli, G. Stoclet, A. Ikeda-Ohno, T. Loiseau, *Chem. Sci.* **2018**, *9*, 5021 – 5032; b) N. P. Martin, C. Volkringer, P. Roussel, J. Marz, C. Hennig, T. Loiseau, A. Ikeda-Ohno, *Chem. Commun.* **2018**, *54*, 10060 – 10063; c) K. E. Knope, N. A. Vanagas, R. F. Higgins, J. N. Wacker, D. Romar, C. Asuigui, E. Warzecha, S. A. Kozimor, S. L. Stoll, E. J. Schelter, J. A. Bertke, *Chem. Eur. J.* **2020**, *26*, 5872 – 5886; d) C. Falaise, C. Volkringer, J. F. Vigier, A. Beaurain, P. Roussel, P. Rabu, T. Loiseau, *J. Am. Chem. Soc.* **2013**, *135*, 15678 – 15681; e) L. Soderholm, P. M. Almond, S. Skanthakumar, R. E. Wilson, P. C. Burns, *Angew. Chem. Int. Ed.* **2008**, *47*, 298 – 302; *Angew. Chem.* **2008**, *120*, 304 – 308.

[8] G. E. Sigmon, A. E. Hixon, *Chem. Eur. J.* **2019**, *25*, 2463 – 2466.

[9] C. Falaise, H. A. Neal, M. Nyman, *Inorg. Chem.* **2017**, *56*, 6591 – 6598.

[10] Y. Suzuki, S. D. Kelly, K. M. Kemner, J. F. Banfield, *Nature* **2002**, *419*, 134.

[11] I. Colliard, G. Morrosin, H. C. zurLoye, M. Nyman, *J. Am. Chem. Soc.* **2020**, *142*, 9039 – 9047.

[12] K. E. Knope, L. Soderholm, *Chem. Rev.* **2013**, *113*, 944 – 994.

[13] a) E. S. Ilton, A. Haiduc, C. L. Cahill, A. R. Felmy, *Inorg. Chem.* **2005**, *44*, 2986 – 2988; b) P. C. Burns, R. J. Finch, *Am. Mineral.* **1999**, *84*, 1456 – 1460.

[14] a) T. Gouder, R. Eloirdi, R. Caciuffo, *Sci. Rep.* **2018**, *8*, 8306; b) C. S. Chen, S. F. Lee, K. H. Lii, *J. Am. Chem. Soc.* **2005**, *127*, 12208 – 12209; c) K. Yuan, D. Renock, R. C. Ewing, U. Becker, *Geochim. Cosmochim. Acta* **2015**, *156*, 194 – 206.

[15] N. Magnani, R. Caciuffo, *Inorganics* **2018**, *6*, 26.

[16] F. Xu, H. N. Miras, R. A. Scullion, D. L. Long, J. Thiel, L. Cronin, *Proc. Natl. Acad. Sci. USA* **2012**, *109*, 11609 – 11612.

[17] A. Vinslava, A. J. Tasiopoulos, W. Wemsdorfer, K. A. Abboud, G. Christou, *Inorg. Chem.* **2016**, *55*, 3419 – 3430.

[18] A. Müller, S. Roy, *Coord. Chem. Rev.* **2003**, *245*, 153 – 166.

[19] P. Frank, R. K. Szilagyi, V. Gramlich, H. F. Hsu, B. Hedman, K. O. Hodgson, *Inorg. Chem.* **2017**, *56*, 1080 – 1093.

[20] A. I. Mishustin, *Russ. J. Inorg. Chem.* **2007**, *52*, 283 – 288.

[21] R. D. Shannon, *Acta Crystallogr. Sect. A Cryst. Phys. Diffr. Theor. Gen. Crystallogr.* **1976**, *32*, 751 – 767.

[22] P. C. Burns, R. C. Ewing, F. C. Hawthorne, *Can. Mineral.* **1997**, *35*, 1551 – 1570.

[23] C. S. Lee, S. L. Wang, K. H. Lii, *J. Am. Chem. Soc.* **2009**, *131*, 15116 – 15117.

[24] C. H. Lin, K. H. Lii, *Angew. Chem. Int. Ed.* **2008**, *47*, 8711 – 8713; *Angew. Chem.* **2008**, *120*, 8839 – 8841.

[25] C. S. Lee, C. H. Lin, S. L. Wang, K. H. Lii, *Angew. Chem. Int. Ed.* **2010**, *49*, 4254 – 4256; *Angew. Chem.* **2010**, *122*, 4350 – 4352.

[26] K. A. Pace, V. V. Klepov, G. Morrison, H. C. Zur Loye, *Chem. Commun.* **2018**, *54*, 13794 – 13797.

[27] S. Duval, S. Sobanska, P. Roussel, T. Loiseau, *Dalton Trans.* **2015**, *44*, 19772 – 19776.

[28] L. R. Ocone, B. P. Block, J. P. Collman, D. A. Buckingham, *Inorg. Synth.* **1966**, 125 – 132.

[29] Bruker AXS Inc., *SAINT Plus Version 8.34a*, Madison, WI, USA, **2013**.

[30] G. M. Sheldrick, *Bruker-Siemens area Detect. Absorpt. other Correct.* Version 2008/12008, **2008**.

[31] G. M. Sheldrick, *Acta Crystallogr. Sect. A Found. Adv.* **2015**, 71, 3 – 8.

[32] G. M. Sheldrick, *Acta Crystallogr. Sect. A Found. Crystallogr.* **2008**, *64*, 112 – 122.

[33] O. V. Dolomanov, L. J. Bourhis, R. J. Gildea, J. A. Howard, H. Puschmann, *J. Appl. Crystallogr.* **2009**, *42*, 339 – 341.

[34] J. Ilavsky, P. R. Jemian, *J. Appl. Crystallogr.* **2009**, *42*, 347 – 353.

[35] M. D. Hanwell, D. E. Curtis, D. C. Lonie, T. Vandermeersch, E. Zurek, G. R. Hutchison, *J. Cheminf.* **2012**, *4*, 17.

Manuscript received: May 15, 2020

Accepted manuscript online: July 1, 2020

Version of record online: September 4, 2020

